

A targeted search for repeating fast radio bursts associated with gamma-ray bursts

Nipuni T. Palliyaguru,^{1,2,†*} Devansh Agarwal,^{3,4} Golnoosh Golpayegani,^{3,4,5}
 Ryan Lynch,^{6,7} Duncan R. Lorimer,^{3,4} Benjamin Nguyen,⁸ Alessandra Corsi¹
 and Sarah Burke-Spolaor^{3,4,9}

¹*Department of Physics and Astronomy, Texas Tech University, Lubbock, TX 79409-1051 (USA)*

²*Arecibo Observatory, HC3 Box 53995, Arecibo, PR 00612*

³*Department of Physics and Astronomy, West Virginia University, Morgantown, WV 26506-6315*

⁴*Center for Gravitational Waves and Cosmology, West Virginia University, Chestnut Ridge Research Building, Morgantown, WV 26505*

⁵*Department of Astronomy, University of California, Berkeley, 501 Campbell Hall #3411, Berkeley, CA, 94720, USA*

⁶*Green Bank Observatory, PO Box 2, Green Bank, WV 24944, USA*

⁷*National Radio Astronomy Observatory, Charlottesville, VA 22903, USA*

⁸*Department of Physics and Astronomy, Franklin and Marshall College, Lancaster, PA 17604, USA*

⁹*CIFAR Azrieli Global Scholars program, CIFAR, Toronto, Canada*

Accepted XXX. Received YYY; in original form ZZZ

ABSTRACT

The origin of fast radio bursts (FRBs) still remains a mystery, even with the increased number of discoveries in the last three years. Growing evidence suggests that some FRBs may originate from magnetars. Large, single-dish telescopes such as Arecibo Observatory (AO) and Green Bank Telescope (GBT) have the sensitivity to detect FRB 121102-like bursts at gigaparsec distances. Here we present searches using AO and GBT that aimed to find potential radio bursts at 11 sites of past γ -ray bursts that show evidence for the birth of a magnetar. We also performed a search towards GW170817, which has a merger remnant whose nature remains uncertain. We place 10σ fluence upper limits of ≈ 0.036 Jy ms at 1.4 GHz and ≈ 0.063 Jy ms at 4.5 GHz for AO data and fluence upper limits of ≈ 0.085 Jy ms at 1.4 GHz and ≈ 0.098 Jy ms at 1.9 GHz for GBT data, for a maximum pulse width of ≈ 42 ms. The AO observations had sufficient sensitivity to detect any FRB of similar luminosity to the one recently detected from the Galactic magnetar SGR 1935+2154. Assuming a Schechter function for the luminosity function of FRBs, we find that our non-detections favor a steep power-law index ($\alpha \lesssim -1.1$) and a large cut-off luminosity ($L_0 \gtrsim 10^{41}$ erg/s).

Key words: gamma-ray burst: general – radio continuum: transients

1 INTRODUCTION

Fast radio bursts (FRBs; Lorimer et al. 2007; Thornton et al. 2013) are millisecond-duration radio pulses with large dispersion measures, generally known to be of cosmological origin (for recent reviews, see Petroff et al. 2019; Cordes & Chatterjee 2019), with the exception of FRBs from the Galactic magnetar SGR1935+2154 (The CHIME/FRB Collaboration et al. 2020; Bochenek et al. 2020). Measurements to date imply total isotropic energies of the order of $\approx 10^{38} - 10^{40}$ erg (Law et al. 2017; Zhang 2018; Dolag et al. 2015), and high brightness temperatures that point to coherent emission processes. So far, there are over 100 known FRBs¹ (Petroff et al. 2016) with ≈ 20 repeating (Spitler et al. 2016; CHIME/FRB Collaboration et al. 2019a,b; Fonseca et al. 2020). Over 50 were found within the last three years by The Australian

Square Kilometre Array Pathfinder (ASKAP; Shannon et al. 2018) and The Canadian Hydrogen Intensity Mapping Experiment (CHIME; CHIME/FRB Collaboration et al. 2018).

Despite this rapid growth in observational results, the origin of FRBs is still uncertain. Theories proposed to explain the origin of FRBs include giant flares from magnetars (Pshirkov & Postnov 2010; Kulkarni et al. 2014; Metzger et al. 2017), giant pulses powered by spin-down from extragalactic neutron stars (NS; Cordes & Wasserman 2016), produced from infalling asteroids to the pulsar’s magnetosphere (Dai et al. 2016), collapse of massive NSs (Falcke & Rezzolla 2014) or compact binary mergers. While there may be multiple classes of FRBs (Palaniswamy et al. 2018), the repeaters rule out catastrophic progenitors, at least for those particular objects. The localization of the repeating FRB 121102 (Spitler et al. 2016) to a low-metallicity dwarf galaxy (Tendulkar et al. 2017; Chatterjee et al. 2017), started pointing to a NS origin for FRBs. The more recent discovery of FRBs from the Galactic source SGR 1935+2154 (The CHIME/FRB

* E-mail: nipuni.palliyaguru@ttu.edu

¹ <http://frbcat.org>

(Collaboration et al. 2020; Bochenek et al. 2020) further confirms this. The idea of a millisecond magnetar, a NS with millisecond birth period and a large magnetic field ($> 10^{15}$ G), being responsible for the FRBs has been put forward since the discovery of FRBs (Pshirkov & Postnov 2010) and recently invoked to explain FRB121102 (Metzger et al. 2017). Connections have also been made previously between FRBs and Soft Gamma Repeaters (SGRs), where the sudden release in magnetic energy that powers the SGR may also produce an FRB (Katz 2016; The CHIME/FRB Collaboration et al. 2020; Bochenek et al. 2020). In SGRs, magnetic reconnection produces a strong magnetic pulse that propagates outwards and interacts with the surrounding gas, which could power a millisecond-duration burst in the radio band (Lyubarsky 2014).

Millisecond magnetars may be born in the core collapse of massive stars and/or in the merger of binary NSs (e.g., Usov 1992; Dai & Lu 1998). The rotational energy of a NS is given by,

$$E_{\text{rot}} \approx 2 \times 10^{52} \text{ erg} \left(\frac{M}{1.4 M_{\odot}} \right) \left(\frac{R}{10 \text{ km}} \right)^2 \left(\frac{P}{1 \text{ ms}} \right)^{-1}. \quad (1)$$

Rapid rotation (periods of milliseconds) gives sufficient rotational energy to power a γ -ray burst (Metzger et al. 2011). Therefore, GRBs with intrinsic energy $< 10^{52}$ erg (which is the maximum rotational energy) may be powered by magnetars. Energy injection from a rapidly rotating magnetar is often invoked to explain the energy in GRBs with a supernova (SN) connection (hereafter called GRB-SNe, Mazzali et al. 2014). By comparing the kinetic energy of the associated SN and the γ -ray energy, Mazzali et al. (2014) shows that a magnetar central engine likely powers all GRB-SNe. In this scenario, the spin-down energy of a highly magnetized NS is deposited in the ejecta.

Evidence for the formation of NSs is also seen in some GRBs as a shallower-than-normal decay in the X-ray light curves (Zhang & Mészáros 2001; Corsi & Mészáros 2009). For some of these GRBs, the central engine could be a magnetar, that did not immediately collapse to a BH, where the spin-down energy is deposited into the ejecta, giving rise to X-ray plateaus (Rowlinson et al. 2013).

A merger that produces a stable NS that is rotationally supported may also quite possibly be a source of repetitive FRBs (Yamasaki et al. 2017). The general picture concerning binary neutron star (BNS) mergers is that the merger produces either a BH or a long-lived NS depending on the EOS and the maximum allowable mass for a NS, M_{max} , which could be more than $2.1 M_{\odot}$ (Cromartie et al. 2020). For BNS total mass of $\approx 1.3 - 1.6 M_{\text{max}}$, prompt collapse to a BH occurs, for masses $\lesssim 1.2 M_{\text{max}}$, a hypermassive NS is formed as an intermediate product, which then loses angular momentum and collapses to a BH (Margalit & Metzger 2017), and for low-mass BNS, an indefinitely long-lived NS may be formed (Margalit & Metzger 2017).

The FRB-GRB connection has also been discussed previously, with FRBs resulting from the collapse of a supermassive NS to a BH (Zhang 2014). Palaniswamy et al. (2014) searched for prompt radio emission coincident with GRBs, but these searches could have suffered from low sensitivity (SEFD > 800 Jy), whereas a typical FRB would have a flux density ≈ 0.5 Jy. Several other campaigns that followed up GRBs in search of FRBs have yielded non-detections (Madi-

son et al. 2019; Men et al. 2019; Hilmarsson et al. 2020). However, Bannister et al. (2012) detected candidate single pulses from GRBs, DeLaunay et al. (2016) identified a γ -ray transient in connection with an FRB, whose high isotropic γ -ray energy may be attributed to a magnetar origin, and Wang et al. (2020) identified a marginal association between FRB 171209 and GRB 110715A. Adding to these, the presence of an SN remnant is one explanation for the large RM and the highly magnetized environment of the FRB121102 (Michilli et al. 2018). Intriguingly, Nicholl et al. (2017) found that FRBs arising predominantly from repetitive sources, i.e. originating from magnetars, occur at a rate of 10^4 Gpc^{-3} , consistent with the rates derived from observations. It is also worthwhile pointing out that the birth rate of non-repeating FRBs ($\sim 2700 \text{ yr}^{-1} \text{ Gpc}^{-3}$) is consistent with the high end of the BNS merger rate (Nicholl et al. 2017; Yamasaki et al. 2017).

Motivated by these ideas, we targeted several relatively nearby GRB sites and the BNS merger GW170817 in search of possible FRB signals. A sensitive telescope like Arecibo should be able to detect FRB121102-like bursts of flux density 1.8 mJy (Palaniswamy et al. 2014) to a distance of up to ≈ 4.8 Gpc. The details of our FRB search observations are presented in Section 2, data analysis in Section 3, present results and place constraints on FRB progenitors in Section 4, and we offer our conclusions in Section 5.

2 OBSERVATIONS

Our target list contains 11 GRBs visible in the Arecibo Observatory (AO) declination range and the BNS merger GW 170817, which was observed with the Green Bank Telescope (GBT). Out of the 11 GRBs, there are six long GRB (lGRB) with SN associations, and five GRBs (one lGRB and four short GRBs; sGRBs) that exhibit plateaus in the X-ray light curve. The target list and their properties are given in Table 1. All GRBs have been localized to a region < 2.5 arcsec by high energy observations, which allows single-dish telescopes with a field-of-view (FoV) of a few arcminutes to cover the entire localization error region at full sensitivity.

Full stokes (or polarization self-and cross-products), 8-bit, high time resolution spectra were recorded at both telescopes. A known pulsar was observed at the start of each observation session to verify the status of instruments. Table 2 lists information about the observation setup for AO and GBT. The dates since the GRB trigger, on which the observations were conducted, are shown in Figure 1.

Arecibo observations were carried out between 2017 December 12:50 UTC and 2018 December 19:55 UTC. Arecibo targets were observed for ~ 0.6 hours on each epoch. A total of 114 hours of observations were obtained on all GRBs, with 1–21 hours on each target at each frequency depending on the LST availability. We note that all of the sources are away from the Galactic plane. Data were recorded using the Puerto Rico Ultimate Pulsar Processing Instrument (PUPPI) at center frequencies of 1380 MHz and 4.5 GHz with a bandwidth of ≈ 600 MHz with 512 frequency channels and sampled at $40.96 \mu\text{s}$.

GBT observations were carried out between 2017 November 02:41 UTC and 2018, July 31:02 UTC on 10 epochs. GW 170817 was observed for ~ 1 hour at each frequency

Table 1. The list of targets. Name, redshift, distance, RA, DEC, galactic coordinates (l and b), expected DM, GRB duration (T_{90}), and the minimum detectable luminosity (L_{\min}) corresponding to S/N= 10 at 1.4 GHz.

Name	Redshift	Distance Mpc	RA (deg)	DEC (deg)	l (deg)	b (deg)	Expected DM (cm^{-3} pc)	Duration (sec)	L_{\min} erg/s
GRB 030329/SN2003dh	0.169	812	10:44:50.03	21:31:18.15	216.98	60.69	264.32	25	1.72×10^{40}
GRB 060218/SN2006aj	0.033	145	03:21:39.69	16:52:01.6	166.92	-32.88	173.08	2100	5.5×10^{38}
GRB 120422A/SN2012bz	0.280	1434	09:07:38.42	14:01:06.0	215.22	36.437	413.64	5.35	5.38×10^{40}
GRB 130427A/SN2013cq	0.340	1795	11:32:32.63	27:41:51.7	206.51	72.50	472.37	162.83	8.44×10^{40}
GRB 130702A/SN2013dx	0.145	687	14:29:14.78	15:46:26.1	11.35	64.63	241.17	59	1.23×10^{40}
GRB 130215A/SN2013ez	0.597	3508	02:53:56.6	13:23:13.2	163.07	-39.76	991.80	65.7	3.22×10^{41}
GRB 130603B	0.356	1894	11:28:48.15	17:04:16.9	236.42	68.42	498.47	0.18	9.39×10^{40}
GRB 140903A	0.351	1863	15:52:03.27	27:36:09.4	44.39	50.12	496.38	0.30	9.09×10^{40}
GRB 051221	0.547	2868	21:54:48.71	16:53:28.2	73.54	-28.58	786.02	1.4	2.15×10^{41}
GRB 100816A	0.803	4529	23:26:57.62	26:34:43.9	100.44	32.57	1396.40	2.9	5.37×10^{41}
GRB 130831A	0.479	2459	23:54:29.91	29:25:47.6	08.33	-31.82	663.84	32.5	1.58×10^{41}
GW170817	0.0098	42	13:09:48.089	-23:22:53.35	308.37	39.29	77.27	2.0	1.06×10^{38}

References: Stanek et al. (2003), Cano et al. (2014), Mazzali et al. (2014), D’Elia et al. (2015), Abbott, et al. (2017) and <https://swift.gsfc.nasa.gov/archive/>. https://swift.gsfc.nasa.gov/archive/grb_table/

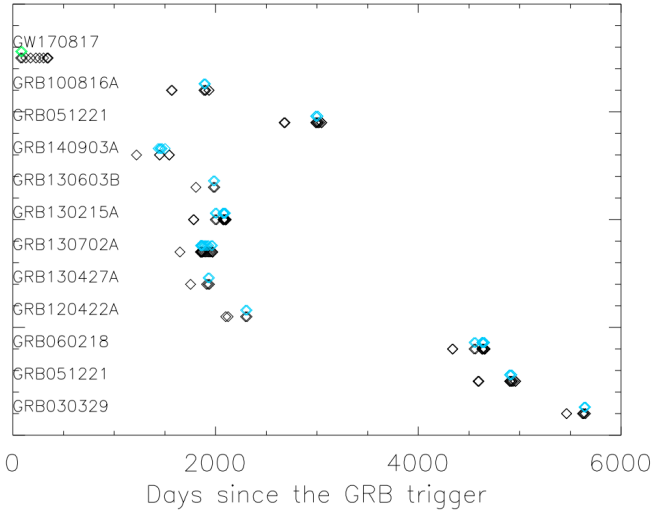


Figure 1. The timescale of our radio observations for the sources that are listed in Table 1 since the GRB trigger. All observations were made within a time span of 412 days, between the dates of November 2, 2017 and December 19, 2018. Our targets are arbitrarily offset along the y-axis for clarity. Black, blue and green diamonds represent 1.4 GHz, 4.5 GHz and 2 GHz observations, respectively. GRB 130702A was monitored \sim once a month in order to verify the origin of an excess dispersion measure seen on the first observation.

during each observation. Since low-frequency emission may be self-absorbed by the post-GRB ejecta at early epochs, observations were conducted at 1.4 and 1.9 GHz on the first two epochs and afterwards only at 1.4 GHz on the following epochs. GBT data were recorded on the GUPPI spectrometer with a sampling time of $10.24 \mu\text{s}$. To minimize any intrachannel dispersive smearing to that caused by the difference between the true and estimated DM, data were semi-coherently dedispersed at a DM of $80 \text{ cm}^{-3} \text{ pc}$. This DM is an estimate corresponding to $\text{DM} = \text{DM}_{\text{MW}} + \text{DM}_{\text{IGM}} + \text{DM}_{\text{H}}$, where $\text{DM}_{\text{MW}} = 35 \text{ cm}^{-3} \text{ pc}$ is the contribution from the Milky Way (Yao et al. 2017), $\text{DM}_{\text{IGM}} = 7 \text{ cm}^{-3} \text{ pc}$, is the intergalactic medium (Ioka 2003), and $\text{DM}_{\text{H}} = 35 \text{ cm}^{-3} \text{ pc}$ is the host galaxy (assuming a host like the MW). We use $\text{DM}_{\text{H}} = 35$

Table 2. Summary of observational setup. Telescope name, center frequency (f_c), System temperature (T_{sys}), Telescope gain, Bandwidth, number of channels (N_{chan}), sampling time (t_{samp}) and the FoV.

Name Telescope	f_c (MHz)	T_{sys} K	Gain (K/Jy)	BW (MHz)	N_{chan}	t_{samp} μs	FoV deg^2
AO	1.4	≈ 30	8	600	512	40.96	9.5×10^{-3}
AO	4.5	≈ 30	4	800	512	40.96	7.8×10^{-4}
GBT	1.4	≈ 20	2.0	800	512	10.24	1.8×10^{-2}
GBT	1.9	≈ 22	1.9	800	512	10.24	8.7×10^{-3}

T_{sys} , Gain and FoV values for AO and GBT are obtained from <http://www.naic.edu/~astro/RXstatus/rcvrtabz.shtml> and <https://science.nrao.edu/facilities/gbt/proposing/GBTpg.pdf> respectively.

$\text{cm}^{-3} \text{ pc}$, which is the approximate DM contribution from the Milky Way for a line of sight out of the plane.

3 DATA ANALYSIS

Data from both telescopes were processed with the GPU accelerated pipeline HEIMDALL² and the PRESTO analysis package (Ransom 2001).

We search the data at the recorded frequency and time resolution using a GPU accelerated pipeline HEIMDALL. The data were dedispersed at $1\text{--}7000 \text{ pc cm}^{-3}$ and were searched for pulse widths of $40.96 \mu\text{s}\text{--}41.93 \text{ ms}$ with the increments in the power of two. This generated 17,672 candidates above S/N of 6. These candidates were then fed to convolutional neural network FETCH³ to classify candidates between radio frequency interference (RFI) and potential FRB candidates (Agarwal et al. 2020). We use model A with a probability threshold of 0.5 for the candidate classification. FETCH labelled 425 candidates as positives. These were inspected manually, 68 candidates were single pulses from the above mentioned test pulsars. The rest of the candidates were false

² <https://sourceforge.net/projects/heimdall-astro/>

³ <https://github.com/devanshkv/fetch>

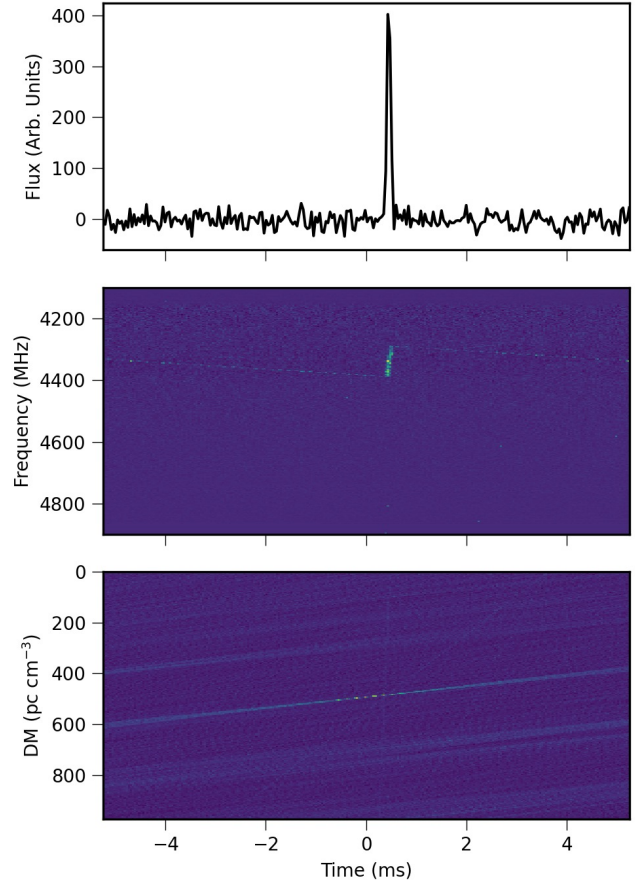
Table 3. GRB name, frequency, total time on the source, the number of epochs observed and the average time duration of each observation.

Name	Frequency (MHz)	Total Time (hours)	Number	Average Time (hours)
GRB 030329	1380	4.5	7	0.65
	4500	1.7	4	0.42
GRB 051221	1380	14.7	15	0.98
	4500	2.5	5	0.51
GRB 060218	1380	8.7	16	0.55
	4500	6.9	13	0.53
GRB 120422A	1380	3.5	4	0.88
	4500	1.2	2	0.60
GRB 130427A	1380	2.7	4	0.67
	4500	1.0	2	0.51
GRB 130702A	1380	13.7	21	0.65
	4500	6.9	15	0.46
GRB 130215A	1380	12.1	19	0.64
	4500	7.5	12	0.63
GRB 130603B	1380	2.3	3	0.76
	4500	1.0	2	0.50
GRB 140903A	1380	4.1	6	0.68
	4500	3.1	6	0.51
GRB 051221	1380	14.7	15	0.98
	4500	2.5	5	0.51
GRB 100816A	1380	5.4	8	0.67
	4500	1.3	3	0.44
GW 170817	1399	8.7	10	0.86
	1999	1.8	2	0.91

positives due to a nearby airport radar. Figure 2 shows an example candidate appearing at a non-zero DM, due to chirped RFI from radar at 4.5 GHz. The appearance of the signal within a narrow band of 4250–4350 MHz confirms the non-astrophysical nature of the signal.

Within PRESTO, RFI excision was done using the tool `rfifind`, which creates a mask in which the affected frequency channels and time chunks are replaced by median values. The data were referenced to the Solar System barycentre and de-dispersed at 1000 trial DMs ranging from 0 to 1000 $\text{cm}^{-3} \text{pc}$. For GRB130215A and GRB100816A, since the expected DM is $> 1000 \text{cm}^{-3} \text{pc}$ (as listed in Table 1), we search 333 trial DMs ranging from 1000 to 2000 $\text{cm}^{-3} \text{pc}$. The dispersion smearing within a channel of $\Delta\nu = 800/512$ MHz at the lowest frequency of 0.98 GHz from this step size is $8.3 \mu\text{s DM } \Delta\nu^{-3} \approx 13.7 \mu\text{s}$, which is negligible.

Significant peaks ($> 10 \sigma$) were searched for, in the de-dispersed time series using the single-pulse pipeline in PRESTO. Each DM vs time plot was visually inspected for real bursts, and those that peaked at a DM of zero were considered as RFI. Candidates that appeared at non-zero DM were reprocessed with `dspsr` (van Straten & Bailes 2011) using the DM and time output by the single-pulse search pipeline in PRESTO, and plotted using PSRCHIVE plotting routines (Hotan et al. 2004). Candidate bursts detected in the single-pulse search were classified as RFI upon further examination.

**Figure 2.** Candidate burst (chirped RFI) from the single-pulse search pipeline in FETCH from GRB 051221 with the brightest signal at $\text{DM} = 486.4 \text{pc cm}^{-3}$. The signal is shown as flux density vs time (top), frequency vs time (middle) and DM vs time (bottom).

4 DISCUSSION

In this section, we discuss the timescales for radiation to escape the GRB ejecta, the possibility of detecting FRBs from magnetars based on the expected flux density and the constraints placed on the luminosity function based on non-detections.

4.1 Detectability of a repeating FRB

The environment of the burst/merger site is an important consideration when determining the timescales for radio emission to escape. The free-free optical depth for the (Oxygen dominated) ejecta would reach $\tau_{\text{eff}} = 1$, on a timescale

$$t = 10 \times \left(93 f_{\text{ion}}^2 \nu_{\text{GHz}}^{-2} T_4^{-3/2} M_{10}^2 t_{10} v_9^{-5} \right)^5 \text{ yr}, \quad (2)$$

after the explosion (Metzger et al. 2017), where f_{ion} is the ionized fraction of the ejecta, ν_{GHz} is the observing frequency, M_{10} is the ejecta mass in units of $10 M_{\odot}$ and T_4 is the ejecta temperature in units of 10^4 K. Assuming ejecta masses of $\sim 10 M_{\odot}$, $f_{\text{ion}} = 0.4$, ejecta velocities $\sim 10^4 \text{km s}^{-1}$, $T_4 = 1$ radio emission may escape after 6 and 3 yr after the explosion

at frequencies 1 GHz and 4.5 GHz respectively. With relatively smaller ejecta masses in mergers (than in SNe), ejecta will be transparent to ~ 1 GHz emission on a timescale of several months (Metzger et al. 2017). This could be as soon as \sim three months for ejecta mass of $\sim 0.001 M_{\odot}$. Our search observations were carried out ≈ 3 months–15 yr after the explosion.

Measured flux densities of bursts from the repeating FRB 121102 were scaled to the distance of each GRB to estimate the expected flux density if a repeater-like source resided in the GRB site. Assuming radiometer noise limitations for each burst, the signal-to-noise ratio

$$S/N = \frac{F G \sqrt{N_p \Delta \nu}}{\beta T_{\text{sys}} \sqrt{w}}, \quad (3)$$

where F is the expected fluence given by $F = S w$ where S is the flux density, $w = 1.0$ ms is the pulse width, T_{sys} is the system temperature, G is the telescope gain (the numbers given in Section 2), $\Delta \nu$ is the bandwidth, $\beta = 1.07$ accounts for digitization loss factors, and $N_p = 2$ is the number of polarizations (Rane et al. 2016). From the radiometer equation, the minimum flux density corresponding to $S/N = 10$ for the AO setup is $S_{\text{min}} \approx 36$ mJy at 1.4 GHz and $S_{\text{min}} \approx 63$ mJy at 4.5 GHz. The minimum flux density for GBT is $S_{\text{min}} \approx 84$ mJy at 1.4 GHz and $S_{\text{min}} \approx 98$ mJy at 1.9 GHz. Figure 3 shows the luminosity distribution and the S/N of 224 bursts at 1.4 GHz and 4–6 GHz from FRB 121102 (Palaniswamy et al. 2014; Hardy et al. 2017; Spitler, et al. 2018; Zhang et al. 2018; Michilli et al. 2018; MAGIC Collaboration et al. 2018; Gourdj, et al. 2019; Hessels et al. 2019). The S/N histograms for bursts when scaled to the distances of two example GRBs from our sample are also shown at 1.4 GHz and 4.5 GHz. The S/N histograms are created by scaling flux density of FRB 121102 bursts to the distances of the GRBs and calculating the ratio between the expected flux density and minimum flux density S_{min} . If magnetars emit FRB121102-like bursts, Arecibo should be able to detect the brightest bursts of luminosity $\approx 9 \times 10^{42}$ erg/s (flux density of 1.8 Jy at 4.5 GHz) at GRB distances up to 4.8 Gpc.

4.2 Luminosity function

In this section, we attempt to place an upper limit on the FRB rate and constrain the FRB luminosity function parameters based on the non-detection of FRBs in our data. The FRB luminosity function may be expressed by the Schechter function (Schechter 1976) where the event rate density per luminosity interval dL is given by

$$\phi(L) dL = \phi^* (L/L_0)^\alpha e^{-L/L_0} d(L/L_0), \quad (4)$$

where ϕ^* is a reference event rate density, α is the power law exponent, and L_0 is the cut-off luminosity.

Following Luo et al. (2020), the event rate above a minimum luminosity L_{min} is then given by,

$$\begin{aligned} R(> L_{\text{min}}) &= \int_{L_{\text{min}}/L_0}^{\infty} \phi^* (L/L_0)^\alpha e^{-(L/L_0)} d\left(\frac{L}{L_0}\right) \\ &= R_0 \Gamma_i \left(\alpha + 1, \frac{L_{\text{min}}}{L_0} \right), \end{aligned} \quad (5)$$

where R_0 is the all-sky event rate in $\text{sky}^{-1} \text{day}^{-1}$, Γ_i is the incomplete gamma function. Here we have replaced the volumetric rate by the all-sky rate. The minimum detectable

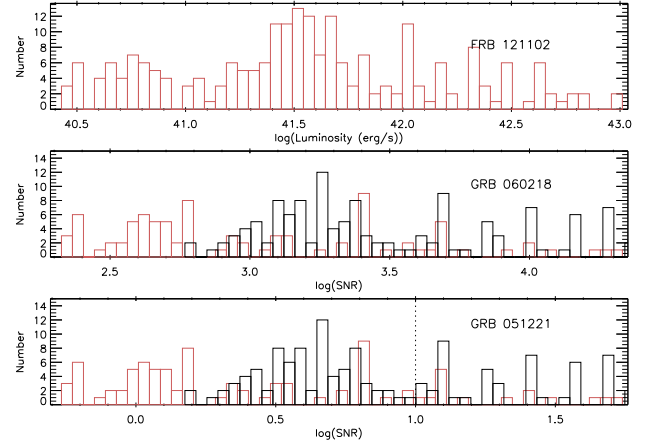


Figure 3. Luminosity distribution of FRB 121102 bursts (top), S/N histograms of GRB 060218 (middle) and GRB 051221 (bottom). The S/N histograms show the S/N at which FRB 121102-like bursts would be detected at given GRB distances. The black dotted vertical line corresponds to $S/N = 10$. The red and black S/N histograms represent bursts at 1.4 GHz and 4.5 GHz respectively.

luminosity at the i^{th} GRB, at a distance D_i , is calculated as $L_{\text{min},i} = 4\pi \Delta \nu S_{\text{min}} D_i^2$. Here, $\Delta \nu$ is the bandwidth and S_{min} is the minimum detectable flux density, calculated from the radiometer equation. The minimum flux density corresponding to $S/N = 10$ for AO and GBT are given in Section 3. Table 1 lists L_{min} values for each GRB at 1.4 GHz. The minimum luminosity of the AO sources at 4.5 GHz is ≈ 2.3 times larger than at 1.4 GHz. The minimum luminosity for GW 170817 at 1.9 GHz is $1.64 \times 10^{38} \text{ erg s}^{-1}$.

If the i^{th} GRB site was searched for T_i days, the expected number of pulses for at that GRB is,

$$n_i = \left(\frac{R T_i \Omega}{41253 \text{ deg}^2} \right). \quad (6)$$

Here, Ω is the FoV of the telescope (listed in Table 2) and T_i is the observation time on the i^{th} source. Therefore, assuming a Poisson distribution of pulses, the probability of observing zero pulses in the i^{th} GRB is, $p_i = e^{-n_i}$. The likelihood of not detecting any GRBs in the entire sample, \mathcal{L} , is the product of all the probabilities, i.e.

$$\mathcal{L} = \prod_{i=1}^N p_i. \quad (7)$$

By summing individual logarithms, we see that

$$\log(\mathcal{L}) = -R_0 \sum_{i=1}^N \Gamma_i \left(\alpha + 1, \frac{L_{\text{min},i}}{L_0} \right) T_i \frac{\Omega}{41253 \text{ deg}^2}. \quad (8)$$

For a given non-detection probability, we can place an upper limit on the all-sky rate and place constraints on the parameters of the luminosity function using Equation 8. Figure 4 shows R_0 vs α and L_0 values for 95% probability. We have combined all data from both AO and GBT.

A millisecond magnetar birth rate of $\approx 170 \text{ Gpc}^{-3} \text{ yr}^{-1}$ and a core-collapse supernova rate of $\approx 2.5 \times 10^5 \text{ Gpc}^{-3} \text{ yr}^{-1}$ (Nicholl et al. 2017), converted to an all-sky rate 0.64 and 937

$\text{sky}^{-1} \text{day}^{-1}$ respectively, are marked by the purple region. To convert the volumetric rate to an all-sky rate we assume that the current AO setup can detect an FRB of 0.19 mJy at 1.4 GHz (mean flux density of FRB 121102; Palaniswamy et al. 2014) up to a distance of ≈ 2.2 Gpc with $S/N = 10$). We also assume a duty cycle of $\eta \approx 0.1$ and a beaming factor of $\xi \approx 0.3$. The sky rate for non-repeating FRBs, scaled to our observations such that $R_0 \approx 1.8 \times 10^4 \text{sky}^{-1} \text{day}^{-1}$ above 36 mJy, is marked by the blue region. Here we use the expression for the all-sky rate

$$R(> S) = R_0 \left(\frac{S}{\text{Jy}} \right)^{\alpha'}, \quad (9)$$

where S is the minimum flux density, $R_0 = 1140 \text{sky}^{-1} \text{day}^{-1}$, is the reference rate at a flux density of 1 Jy and $\alpha' = -0.83$ is the source count index (Agarwal et al. 2020) from the log N-log S relation (Lawrence et al. 2017). To be consistent with the expected rates of millisecond magnetar formation, L_0 should be higher for smaller α (purple region). In general $\alpha \lesssim -1.1$ and $L_0 \gtrsim 10^{41} \text{erg s}^{-1}$.

Luo et al. (2020) finds from real FRBs luminosity function parameters $L_0 = 2.9^{+11.9}_{-1.7} \times 10^{44} \text{erg s}^{-1}$, $\alpha = -1.79^{+0.31}_{-0.35}$ and a volumetric rate of $\phi^* = 339 \text{Gpc}^{-3} \text{yr}^{-1}$. This corresponds to an all-sky rate of $R_0 \approx 42.4 \text{sky}^{-1} \text{day}^{-1}$ at 1.4 GHz. From Figure 4, and Equation 8 we find that for $L_0 = 2.9 \times 10^{44} \text{ergs}^{-1}$ and $\alpha = -1.79$ gives $R_0 \approx 2.4 \text{sky}^{-1} \text{day}^{-1}$, above a flux density of 36 mJy. A flat spectrum for FRBs is assumed here. We further note that the all-sky FRB rate for repeaters will be a fraction of this rate.

Recent studies have shown that FRB 121102 shows a periodicity and clustering and therefore the burst distribution may be better described by a Weibull distribution than a Poisson distribution (Oppermann et al. 2018). However, this may be the effect of a few strongly clustered bursts and the burst distribution may still be Poissonian (Cruces et al. 2020). The non-detection probability for a Weibull distribution is given by (Oppermann et al. 2018)

$$p = \frac{\Gamma(1/k) \Gamma_i(1/k, (T_i r \Gamma(1 + 1/k))^k)}{k \Gamma(1 + 1/k)} \quad (10)$$

where k is the shape parameter which describes the degree of clustering, r is the burst rate, T_i is the observation time, Γ is the Gamma function, Γ_i is the incomplete Gamma function. For $k = 1$ the Weibull distribution becomes a Poisson distribution and for $k < 1$ clustering with small intervals is favoured (Oppermann et al. 2018). Considering a burst rate of $r = 5.7 \text{day}^{-1}$ (Oppermann et al. 2018) and scaling the rate to the distance of each GRB, and taking the product of probabilities for each GRB, the total non-detection probability for AO observations is 3.9×10^{-6} for a Poisson process. For a Weibull distribution with $k = 0.34$ (Oppermann et al. 2018), the non-detection probability is 1.8×10^{-5} . Here we ignore GRB 060218, since it has a high rate and hence a very small non-detection probability.

5 CONCLUSION

We conducted a single-pulse search for FRBs from 12 well-localized targets that show evidence for magnetar formation. The target list includes six GRB-SNe, four sGRBs, one IGRB without a SN association, and GW170817, for

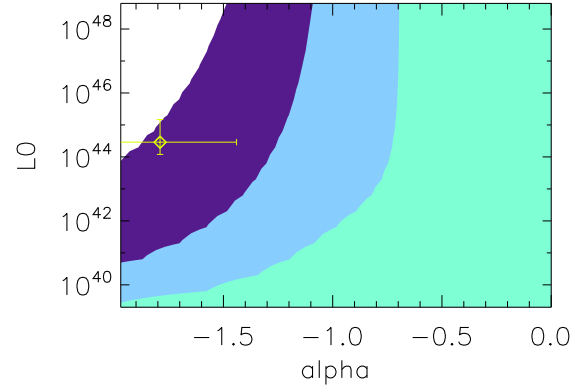


Figure 4. R_0 vs L_0 and α for Schechter function for 95% non-detection probability. The white, purple, light blue, and aqua green regions correspond to $R_0 \lesssim 0.64 \text{sky}^{-1} \text{day}^{-1}$, between 0.64 and $937 \text{sky}^{-1} \text{day}^{-1}$, between 937 and $1.8 \times 10^4 \text{sky}^{-1} \text{day}^{-1}$, and $\gtrsim 1.8 \times 10^4 \text{sky}^{-1} \text{day}^{-1}$, respectively. Luo et al. (2020) LF parameters of $L_0 = 2.9^{+11.9}_{-1.7} \times 10^{44} \text{erg/s}$ and $\alpha = -1.79^{+0.35}_{-0.31}$ are marked by a yellow diamond.

which the merger remnant is undetermined. These searches were conducted ~ 3 months–15 years after the explosion. We show that large single-dish telescopes are well suited to detect FRBs from such extragalactic targets at Gpc distances. Our searches resulted in candidates that were confirmed to be either RFI or single pulses from the known test pulsars. Our constraints on the FRB luminosity function parameters, based on non-detection, are consistent with published values.

The detection of a late-time FRB signal from a GRB site would undoubtedly be the smoking gun signature of magnetar birth which would have a tremendous scientific impact with vast implications for fundamental physics and cosmology for this decade (Law et al. 2019). New wide-field radio telescopes have more than doubled the number of FRBs over the last two years. However, even with the increased number of bursts in the last two years, mechanisms that produce FRBs remain a mystery. Determining the observing cadence remains one of the main challenges in targeted searches. If FRBs are indeed related to explosive events, a better understanding of the emission process and the environment of the explosion will help determine factors such as time for radiation to escape and thereby an observing cadence for future targeted searches. Novel techniques to catch possible radio bursts from gravitational wave counterparts are emerging (Clancy et al. 2019). Better algorithms that reduce the number of candidates and distinguish between RFI and real transients are also in place. Furthermore, even though radio telescopes with large fields-of-view is dominating FRB searches, sensitive single-dish telescopes will continue to play a crucial role in follow-up searches at targeted locations.

ACKNOWLEDGEMENTS

NTP thanks the Phill Perrillat, Hector Hernandez and other Arecibo Observatory staff for data quality checks, schedul-

ing and support with observing. We thank Akshaya Rane, Jayanth Chennamangalam, Andrew Seymour and Scott Ransom for help with observations and data processing issues. The Arecibo Observatory is a facility of the National Science Foundation operated under cooperative agreement by the University of Central Florida in alliance with Yang Enterprises, Inc. and Universidad Metropolitana. The Green Bank Observatory is a facility of the National Science Foundation operated under cooperative agreement by Associated Universities, Inc. A. Corsi acknowledges support from NSF Award #1907975. DRL acknowledges support from the NSF awards AAG-1616042, OIA-1458952 and PHY-1430284. SBS acknowledges support from NSF grant AAG-1714897. SBS is a CIFAR Azrieli Global Scholar in the Gravity and the Extreme Universe program.

DATA AVAILABILITY

The data underlying this article will be shared on reasonable request to the corresponding author.

REFERENCES

- Abbott B. P., et al. 2017, *ApJL*, 848, L12
- Agarwal, D., Aggarwal, K., Burke-Spolaor, S., et al. 2020, *MNRAS*, doi:10.1093/mnras/staa1856
- Agarwal, D., Lorimer, D. R., Surnis, M. P., et al. 2020, *MNRAS*, arXiv:2003.14272
- CHIME/FRB Collaboration, Amiri, M., Bandura, K., et al. 2018, *ApJ*, 863, 48
- CHIME/FRB Collaboration, Amiri, M., Bandura, K., et al. 2019, *Nature*, 566, 235
- CHIME/FRB Collaboration, Andersen, B. C., Bandura, K., et al. 2019, *ApJ*, 885, L24
- Fonseca, E., Andersen, B. C., Bhardwaj, M., et al. 2020, *ApJ*, 891, L6
- The CHIME/FRB Collaboration, ;, Anderson, et al. 2020, arXiv:2005.10324
- Bannister, K. W., Murphy, T., Gaensler, B. M., & Reynolds, J. E. 2012, *ApJ*, 757, 38
- Bochenek, C. D., McKenna, D. L., Belov, K. V., et al. 2020, *PASP*, 132, 034202
- Champion, D. J., Petroff, E., Kramer, M., et al. 2016, *MNRAS*, 460, L30
- Cano, Z., de Ugarte Postigo, A., Pozanenko, A., et al. 2014, *A&A*, 568, A19
- Chatterjee, S., Law, C. J., Wharton, R. S., et al. 2017, *Nature*, 541, 58
- Cordes, J. M., & Wasserman, I. 2016, *MNRAS*, 457, 232
- Cordes, J. M., & Chatterjee, S. 2019, *ARA&A*, 57, 417
- Corsi, A., & Mészáros, P. 2009, *ApJ*, 702, 1171
- Cromartie, H. T., Fonseca, E., Ransom, S. M., et al. 2020, *Nature Astronomy*, 4, 72
- Cruces, M., Spitler, L. G., Scholz, P., et al. 2020, arXiv:2008.03461
- Dai, Z. G., & Lu, T. 1998, *A&A*, 333, L87
- Dai, Z. G., Wang, J. S., Wu, X. F., & Huang, Y. F. 2016, *ApJ*, 829, 27
- D’Elia, V., Pian, E., Melandri, A., et al. 2015, *A&A*, 577, A116
- Dainotti, M. G., Hernandez, X., Postnikov, S., et al. 2017, arXiv:1704.04908
- DeLaunay, J. J., Fox, D. B., Murase, K., et al. 2016, *ApJ*, 832, L1
- Dolag, K., Gaensler, B. M., Beck, A. M., & Beck, M. C. 2015, *MNRAS*, 451, 4277
- Falcke, H., & Rezzolla, L. 2014, *AA*, 562, A137
- Gourdji K., Michilli D., Spitler L. G., Hessels J. W. T., Seymour A., Cordes J. M., Chatterjee S., 2019, *ApJL*, 877, L19
- Hessels, J. W. T., Spitler, L. G., Seymour, A. D., et al. 2019, *ApJ*, 876, L23
- Hilmarsson, G. H., Spitler, L. G., Keane, E. F., et al. 2020, *MNRAS*, 493, 5170
- Hotan, A. W., van Straten, W., & Manchester, R. N. 2004, *PASA*, 21, 302
- Hardy, L. K., Dhillon, V. S., Spitler, L. G., et al. 2017, *MNRAS*, 472, 2800
- Ioka, K. 2003, *ApJ*, 598, L79
- Katz, J. I. 2016, *ApJ*, 826, 226
- Kisaka, S., & Ioka, K. 2015, *ApJ*, 804, L16
- Law, C. J., Abruzzo, M. W., Bassa, C. G., et al. 2017, *ApJ*, 850, 76
- Law, C. J., Margalit, B., Palliyaguru, N. T., et al. 2019, arXiv:1903.04691
- Lawrence, E., Vander Wiel, S., Law, C., et al. 2017, *AJ*, 154, 117
- Luo, R., Men, Y., Lee, K., et al. 2020, *MNRAS*, 494, 665
- Lyubarsky, Y. 2014, *MNRAS*, 442, L9
- Kulkarni, S. R., Ofek, E. O., Neill, J. D., Zheng, Z., & Juric, M. 2014, *ApJ*, 797, 70
- Lorimer, D. R., Bailes, M., McLaughlin, M. A., Narkevic, D. J., & Crawford, F. 2007, *Science*, 318, 777
- Madison, D. R., Agarwal, D., Aggarwal, K., et al. 2019, *ApJ*, 887, 252
- MAGIC Collaboration, Acciari, V. A., Ansoldi, S., et al. 2018, *MNRAS*, 481, 2479
- Margalit, B., & Metzger, B. D. 2017, *ApJ*, 850, L19
- Mazzali, P. A., McFadyen, A. I., Woosley, S. E., Pian, E., & Tanaka, M. 2014, *MNRAS*, 443, 67
- Men, Y., Aggarwal, K., Li, Y., et al. 2019, *MNRAS*, 489, 3643
- Metzger, B. D., Giannios, D., Thompson, T. A., Bucciantini, N., & Quataert, E. 2011, *MNRAS*, 413, 2031
- Metzger, B. D., Berger, E., & Margalit, B. 2017, *ApJ*, 841, 14
- Michilli, D., Seymour, A., Hessels, J. W. T., et al. 2018, *Nature*, 553, 182
- Nicholl, M., Williams, P. K. G., Berger, E., et al. 2017, *ApJ*, 843, 84
- Oppermann, N., Yu, H.-R., & Pen, U.-L. 2018, *MNRAS*, 475, 5109
- Palaniswamy, D., Wayth, R. B., Trott, C. M., et al. 2014, *ApJ*, 790, 63
- Palaniswamy, D., Li, Y., & Zhang, B. 2018, *ApJ*, 854, L12
- Petroff, E., Barr, E. D., Jameson, A., et al. 2016, *Publ. Astron. Soc. Australia*, 33, e045
- Petroff, E., Hessels, J. W. T., & Lorimer, D. R. 2019, *A&ARv*, 27, 4
- Popov, S. B., & Postnov, K. A. 2010, *Evolution of Cosmic Objects through their Physical Activity*, 129
- Pshirkov, M. S., & Postnov, K. A. 2010, *Ap&SS*, 330, 13
- de Ugarte Postigo, A., Thöne, C. C., Rowlinson, A., et al. 2014, *A&A*, 563, A62
- Rane, A., Lorimer, D. R., Bates, S. D., et al. 2016, *MNRAS*, 455, 2207
- Ransom, S. M. 2001, Ph.D. Thesis,
- Ravi, V., Battaglia, N., Burke-Spolaor, S., et al. 2019, arXiv:1903.06535
- Rowlinson, A., O’Brien, P. T., Metzger, B. D., Tanvir, N. R., & Levan, A. J. 2013, *MNRAS*, 430, 10
- Shannon, R. M., Macquart, J.-P., Bannister, K. W., et al. 2018, *Nature*, 562, 386
- Spitler, L. G., Scholz, P., Hessels, J. W. T., et al. 2016, *Nature*, 531, 202
- Spitler L. G., et al., 2018, *ApJ*, 863, 150
- Stanek, K. Z., Matheson, T., Garnavich, P. M., et al. 2003, *ApJ*, 591, L17
- Tendulkar, S. P., Bassa, C. G., Cordes, J. M., et al. 2017, *ApJ*, 834, L7

- Thompson, C., & Duncan, R. C. 1995, MNRAS, 275, 255
Thornton, D., Stappers, B., Bailes, M., et al. 2013, Science, 341, 53
Usov, V. V. 1992, Nature, 357, 472
van Straten, W., & Bailes, M. 2011, Publ. Astron. Soc. Australia, 28, 1
Wang, X.-G., Li, L., Yang, Y.-P., et al. 2020, ApJ, 894, L22
Yamasaki, S., Totani, T., & Kiuchi, K. 2017, arXiv:1710.02302
Yao, J. M., Manchester, R. N., & Wang, N. 2017, ApJ, 835, 29
Zhang, B., & Mészáros, P. 2001, ApJ, 552, L35
Zhang, B.-B., Fan, Y.-Z., Shen, R.-F., et al. 2012, ApJ, 756, 190
Zhang, B. 2014, ApJ, 780, L21
Zhang, B. 2018, arXiv:1808.05277
Zhang Y. G., Gajjar V., Foster G., Siemion A., Cordes J., Law C., Wang Y., 2018, ApJ, 866, 149